

Noise-resilient voltage and frequency synchronisation of an autonomous microgrid

ISSN 1751-8687

Received on 20th August 2018

Revised 27th September 2018

Accepted on 3rd October 2018

E-First on 18th December 2018

doi: 10.1049/iet-gtd.2018.6409

www.ietdl.org

Sonam Shrivastava¹, Bidyadhar Subudhi¹ ✉, Susmita Das²

¹Department of Electrical Engineering, Centre for Renewable Energy Systems, National Institute of Technology Rourkela, Rourkela 769008, India

²Department of Electrical Engineering, National Institute of Technology Rourkela, Rourkela 769008, India

✉ E-mail: bidyadhar@nitrrkl.ac.in

Abstract: We present a new noise-resilient secondary control scheme for voltage and frequency synchronisation of an autonomous microgrid (MG). The communication network is an integral part of distributed secondary control structure. The communication links among the distributed generator units are assumed to be ideal in nature. However, the communication links are subjected to uncertain noises, which can significantly affect the synchronisation performance of MG control. We consider the information received over the communication link is corrupted with generalised Gaussian noise. Further, the complete non-linear model of the MG system has been considered for designing a robust distributed control scheme augmented with an auxiliary corrective control input to counterbalance the impact of noises. The performance of the proposed control scheme is evaluated by pursuing simulation of a MG test system in MATLAB/SimPoweSystem environment under load perturbation, changes in communication topology, communication link delays, data dropout, and variations in noise parameter. The results of a comparative assessment of the proposed control scheme with two approaches first a neighbourhood tracking error-based control scheme and second a noise-resilient control scheme are presented to illustrate the effectiveness of the proposed robust noise-resilient control scheme in voltage and frequency synchronisation and accurate active power-sharing.

Nomenclature

\mathcal{G}	weighted, undirected, and connected communication graph
$A_{\mathcal{G}}$	adjacency matrix of communication graph
$\mathcal{L}_{\mathcal{G}}$	Laplacian matrix of communication graph
λ_i	eigenvalues of Laplacian matrix
N	number of DG units (nodes) in microgrid network
N_L	number of leader nodes
N_F	number of follower nodes
x_i	state vector for the i^{th} DG dynamics
V_i	output voltage of the i^{th} DG unit
ω_i	operating angular frequency of the i^{th} DG unit
V_{ni}	primary control voltage set point
ω_{ni}	primary control angular frequency set point
V_{ref}	nominal voltage value
ω_{ref}	nominal angular frequency value
P_i	active output power of the i^{th} DG unit
Q_i	reactive output power of the i^{th} DG unit
$\delta(t)$	communication noise signal
σ^2	variance noise signal
$u_i^V(u_i^\omega)$	voltage (frequency) control input for the i^{th} DG unit
τ_d	communication link latency

1 Introduction

1.1 Motivation and incitement

The rapidly increasing renewable energy sources (RESs) penetration into the modern electric power system leads to various challenges, e.g. reliability and power quality and so on. Microgrid (MG) has emerged as a promising solution to facilitate the effective deployment and management of these RESs [1–5]. The MG can function in both grid-tied mode and autonomous mode. In the grid-tied operation, the main grid supports the voltage and frequency stabilities, whereas in autonomous operation, when MG is isolated from the main grid due to scheduled maintenance or unpredictable

disturbances, the control task becomes more challenging. A hierarchical control structure has been reported in the literature [6–8] for achieving stable operation of an autonomous MG. This control structure mainly comprises three control layers namely primary, secondary, and tertiary controls. The primary control is implemented locally via a droop control scheme in a distributed manner to maintain voltage and frequency stabilities of distributed generator (DG) units in MG network. Despite the simple implementation, the droop control scheme results in voltage and frequency deviations from the reference values. The secondary control is therefore imperative to synchronise the voltage and frequency to their nominal values. The tertiary control layer provides the cost and power flow optimisation over the MG network [9].

1.2 Literature review

Several researchers have extensively studied the secondary control level of MG network. For example, traditional secondary control employs the centralised structure, that necessitates the use of a central computing unit and complex communication network, hence increases the computational burden and affects flexibility and reliability of the MG system. Thus, the system is likely to encounter a single-point-failure [10, 11]. However, the distributed secondary control overcomes these drawbacks and increases the system reliability. The distributed control approaches are inspired by the networked control of multi-agent system (MAS) and spatially dispersed DG units, which uses only the neighbours' information. Several distributed control structures have been reported in the literature which utilises neighbouring information and can be implemented over a cost-efficient sparse communication network [12–18]. A feedback linearisation approach has been proposed in [12, 18] to reduce the non-linear system into a linear system and convert the distributed voltage control into a tracking synchronisation problem. Further, in [17], a droop-free control scheme is employed for voltage and frequency restoration, but it makes the system vulnerable to communication network failure. A frequency and active power regulation scheme

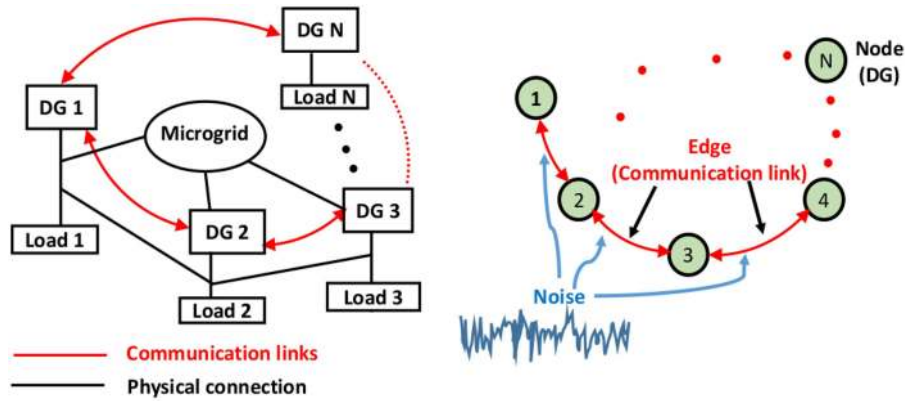


Fig. 1 Noisy communication links in cyber physical MG
 (a) Physical MG network, (b) Information exchange over noisy communication links

is presented in [19], and the results show that the performance of the controller deteriorates with change in communication topology, link failure, data dropout, and time-delays. The communication network plays an important role in the secondary control implementation. Further, various communication constraints such as fixed and time-varying communication link delays, link breakage and so on are addressed in [20–22].

The cyber-physical structure of MG is shown in Fig. 1. The information exchange among the DG units with noise uncertainty is shown in the cyber layer, and the physical layer shows the inverter-based DG units with lines and loads. The existing distributed secondary control schemes are augmented with the communication layer and assume the ideal, noise-free communication among the DG units. However, in practical scenarios, the communication links are corrupted with noises arising out from the sensor uncertainty, and malicious attack or environmental cause, e.g. rain. This noise can be modelled as generalised Gaussian noise with zero mean, i.e. white noise [23]. The noisy measurement data can adversely affect the sensitive electronic devices and further results in instability of the MG network. One of such cases of noisy environment is considered in [24, 25] where a leader–follower consensus approach for tracking in a MAS is presented. A similar problem is also considered in [26] that employs distributed least mean square algorithm only for voltage and frequency regulation and does not provide any comment on power regulation. A distributed noise resilient secondary control scheme is proposed in [27], but high oscillations are observed during small-signal (load perturbation) and large-signal disturbances (loss of DG unit).

1.3 Contribution and paper organisation

Having pursued the literature review, we can conclude that there is still an urge for investigation of a noise resilient secondary control paradigm exploiting the sparse communication network. In this paper, we proposed a distributed control scheme for voltage and frequency synchronisation of an autonomous MG while considering noisy communication links. Here, we assumed that the locally measured information is corrupted with additive Gaussian noise and the local primary controller at each DG unit terminal receives the noisy information from their neighbouring DGs. Further, the detailed non-linear system dynamics of MG network is considered for designing the proposed control scheme, that counteracts the noisy measurement via an auxiliary corrective control input and synchronises the voltage and frequency to their nominal values while providing accurate active power sharing. The contributions of the paper can be summarised as follows:

- Unlike the secondary control schemes reported in [12–18], here we consider a practical perspective by incorporating the noisy local measurements from the communication link. Further, we propose a noise-resilient control scheme for voltage and frequency synchronisation and accurate real power-sharing.

- Several existing works consider incomplete system model which affect the performance and stability of designed controllers. In this paper, we consider a complete nonlinear system model with un-modelled dynamics and uncertain noise parameters to design a noise-resilient control scheme which is independent of DG unit parameters such as loads, lines, and specific noise type and noise parameters.
- The proposed control scheme is fully distributed and can be implemented over a low-cost sparse communication network, thereby enabling the plug and play capabilities of the MG network, which is desirable because of the intermittent nature of the RES based DGs.
- Compared with the existing distributed controllers in [12, 18], the proposed noise resilient control scheme reaches consensus rapidly and exhibits robust performance for small-signal (load perturbation) and large-signal disturbances (loss of DG unit), change in communication network topology, and variations in noise parameters.

The remaining of the paper is organised as follows. Section 2 describes the preliminaries of graph theory, modelling and primary control of inverter-based i^{th} DG unit and Gaussian communication noise. The proposed distributed noise resilient voltage and frequency synchronisation schemes are presented in Sections 3 and 4, respectively. Case studies for the performance analysis of the proposed schemes based on the offline time-domain simulations are presented in Section 5. Section 6 concludes the paper.

2 Preliminaries

2.1 Notations

The standard notations \mathbb{R} , \mathbb{R}_n , $\mathbb{R}_{n \times n}$, \mathbb{R}_+ , \mathbb{P}_n , and \mathbb{N}_n denote the set of real numbers; set of real column vector of $n \times 1$; set of $n \times n$ real matrices; set of positive real numbers; set of real positive definite matrices of $n \times n$, and set of non-negative definite matrices of $n \times n$, respectively. $\mathbf{1}_N$, $\mathbf{0}_N$, $(\cdot)^T$, $(\cdot)^{-1}$, and \otimes denote the $n \times 1$ vectors of all ones; $n \times 1$ vectors of all zeroes; transpose; inverse, and Kronecker product [28].

2.2 Algebraic graph theory

We adapted the graph theory notation from [29]. A weighted, undirected and connected graph can be defined as $\mathcal{G} = (\mathcal{V}_{\mathcal{G}}, E_{\mathcal{G}}, \mathbf{A}_{\mathcal{G}})$, where $\mathcal{V}_{\mathcal{G}}$ is node set $\{1, \dots, N\}$, $E_{\mathcal{G}}$ is edge set, i.e. $E_{\mathcal{G}} \subseteq (\mathcal{V}_{\mathcal{G}} \times \mathcal{V}_{\mathcal{G}})$, $\mathbf{A}_{\mathcal{G}}$ is weighted adjacency matrix $\mathbf{A}_{\mathcal{G}} \in \mathbb{R}_{N \times N}$. For an edge $(i, j) \in E_{\mathcal{G}}$, $a_{ij} = a_{ji} = 1$, else $a_{ij} = a_{ji} = 0$. The degree matrix of graph \mathcal{G} is defined as $\mathcal{D} = \text{Diag}\{d_i\} \in \mathbb{R}_{N \times N}$, with $d_i = \sum_{j \in \mathcal{N}_i} a_{ij}$. \mathcal{N}_i is the set of neighbours defined as $\mathcal{N}_i = \{j \in \mathcal{V}_{\mathcal{G}} : (i, j) \in E_{\mathcal{G}}, j \neq i\}$. The Laplacian matrix $\mathcal{L}_{\mathcal{G}} = \mathcal{D} - \mathbf{A}_{\mathcal{G}}$. The spectrum of the graph can be

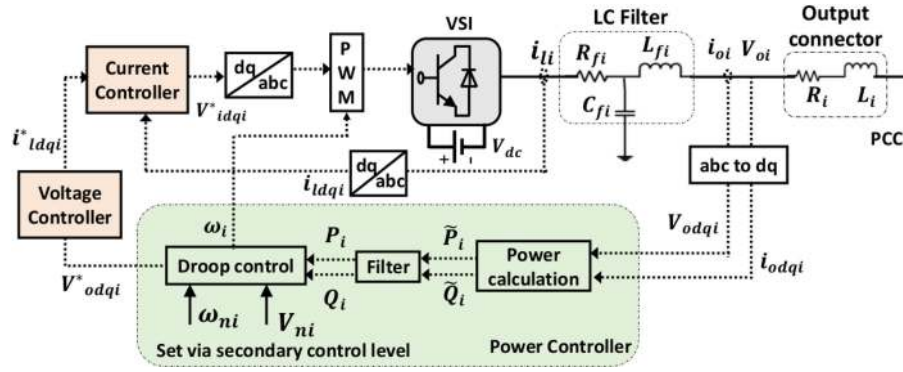


Fig. 2 Block diagram of the inverter-based i th DG unit

given as $0 = \lambda_1 \leq \lambda_2 \leq \dots \leq \lambda_N$. Define $\mathcal{B}_{\mathcal{G}}$ as the incidence matrix of graph \mathcal{G} , with

$$[\mathcal{B}_{\mathcal{G}}]_{ij} = \begin{cases} 1, & \text{if node } i \text{ is the head of edge } j, \\ -1, & \text{if node } i \text{ is the tail of edge } j, \\ 0, & \text{otherwise.} \end{cases}$$

Further, partitioning $N = N_L + N_F$, where N_L and N_F are the number of leader and follower DG units. The graph Laplacian matrix can be partitioned as

$$\mathcal{L}_{\mathcal{G}} = \mathcal{B}_{\mathcal{G}} \mathcal{B}_{\mathcal{G}}^T = \begin{bmatrix} L_{\mathcal{G}} & G_{\mathcal{G}}^T \\ G_{\mathcal{G}} & \mathcal{F}_{\mathcal{G}} \end{bmatrix}$$

where $L_{\mathcal{G}} = \mathcal{B}_{L_{\mathcal{G}}} \mathcal{B}_{L_{\mathcal{G}}}^T$, $G_{\mathcal{G}} = \mathcal{B}_{\mathcal{F}_{\mathcal{G}}} \mathcal{B}_{\mathcal{F}_{\mathcal{G}}}^T$, and $\mathcal{F}_{\mathcal{G}} = \mathcal{B}_{\mathcal{F}_{\mathcal{G}}} \mathcal{B}_{L_{\mathcal{G}}}^T$, where $\mathcal{F}_{\mathcal{G}} \in \mathbb{P}_{N_{\mathcal{F}}}$ [30].

2.3 Primary control of inverter-based i th DG unit

The typical MG network consists of electrical layer, control layer and communication layer. In the electrical layer, DG units comprise of prime DC source, voltage source inverter, series LC filter, RL connector, and loads. The control layer of DG mainly has three control loops namely voltage, current, and power control loops. The dynamical model of DG unit with its inner control loops is adopted from [13] as follows:

$$\frac{dx_i}{dt} = f_i(x_i) + g_{iV}(x_i)u_i^V \quad (1)$$

$$+ g_{i\omega}(x_i)u_i^{\omega} + k_i(x_i)D_i \quad (2)$$

$$y_{iV} = h_{iV}(x_i) = V_i \quad (2)$$

$$y_{i\omega} = h_{i\omega}(x_i) + d_i u_i^{\omega} = \omega_i = \omega_{ni} - k_{P_i}^{\omega} P_i \quad (3)$$

where $x_i = [\alpha_i, P_i, Q_i, i_{di}, i_{qi}, V_{odi}, V_{oqi}, i_{odi}, i_{oqi}]^T$. Fig. 2 shows the general layout of inverter-based MG in islanded operating mode. Distributed droop control scheme is generally used for primary control of DGs and can be given as

$$\omega_i = \omega_{ni} - k_{P_i}^{\omega} P_i \quad (4)$$

$$V_i = V_{ni} - k_{Q_i}^V Q_i \quad (5)$$

where V_i and ω_i are the output voltage magnitude and operating frequency of DG unit, respectively, V_{ni} and ω_{ni} are the primary control set points, Q_i and P_i are the reactive power and active powers, respectively, $k_{Q_i}^V$ and $k_{P_i}^{\omega}$ are the voltage and frequency droop coefficients, respectively. It should be noted that $V_i = \sqrt{V_{odi}^2 + V_{oqi}^2}$, and the primary control scheme aligns the output voltage magnitude on the d -axis, i.e. $V_{odi} = V_i$, by making the q -

axis component zero, i.e. $V_{oqi} = 0$. The primary control scheme results in voltage and frequency deviations, therefore secondary control scheme is employed to restore them to their nominal values, i.e.

$$\omega_i(t) = \omega_j(t) = \omega_{nom}, \quad \forall i, j \quad (6)$$

$$V_i(t) = V_j(t) = V_{nom}, \quad \forall i, j. \quad (7)$$

2.4 Communication noise

The communication structure is an integral part of distributed secondary control. The communication links for information sharing may be affected by the noise due to sensor uncertainty, malicious attacks, and environmental events, i.e. rain. In this paper, we consider that the generalised zero-mean Gaussian noise corrupts the information shared over the communication links. The generalised probability distribution function (PDF) of the considered noise can be given as [31]

$$p(\delta(t)) = \frac{1}{\sqrt{2\pi\sigma^2}} \exp\left(-\frac{1}{2\sigma^2}(\delta(t) - \text{mean}(\delta(t)))^2\right) \quad (8)$$

where σ^2 is the variance of noise signal $\delta(t)$. Considering zero mean and different variance the PDF of noise are shown in Fig. 3.

3 Noise-resilient voltage synchronisation

In this section, a distributed noise-resilient secondary voltage synchronisation scheme is proposed, which employs only neighbours' information and is independent of the type of noise. First, we apply a feedback linearisation approach presented in [12], to obtain a linear system and then the proposed noise resilient secondary control scheme is presented.

3.1 Feedback linearisation

The input output feedback linearisation is employed to transform the non-linear system dynamic of each DG in (1) into a linear system. The linear dynamics of the i th DG can be written as

$$\ddot{y}_{iV} = L_f^2 h_{iV} + L_g L_f h_{iV} U_i \quad (9)$$

where $L_f h_{iV}$ is the Lie derivative of h_{iV} along f_i , y_i is the output (V_i) and U_i denotes the voltage control input. The first derivative of y_{iV} can be written as

$$\dot{y}_{iV} = y_{iV,1} \quad (10)$$

$$\dot{y}_{iV,1} = f_i(x_i) + g_i(x_i)U_i, \quad \forall i \quad (11)$$

Let the auxiliary control input $u_i^V = f_i(x_i) + g_i(x_i)U_i$, then (10) can be written as

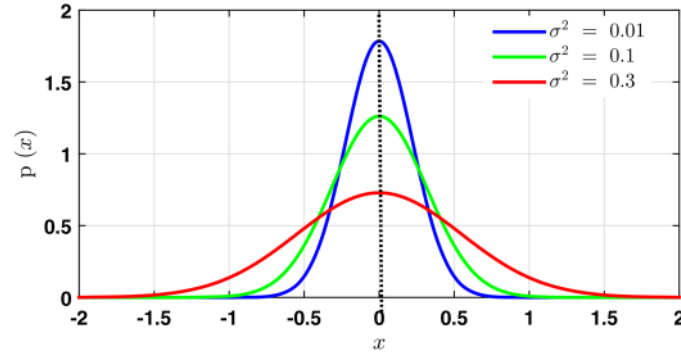


Fig. 3 Probability distribution function of Gaussian noise variance σ_2

$$\dot{y}_{iV} = y_{iV,1} \quad (12)$$

$$\dot{y}_{iV,1} = u_i^V, \forall i \quad (13)$$

Equation (12) can be rewritten in matrix form as follows:

$$\dot{y}_{iV} = Ay_{iV} + Bu_i^V, \quad \forall i \quad (14)$$

where

$$y_{iV} = [y_{iV} y_{iV,1}]^T, \quad B = [0 \ 1]^T \quad \text{and} \\ A = \begin{bmatrix} 0 & 1 \\ 0 & 0 \end{bmatrix}.$$

The leader dynamics can be given as

$$\dot{y}_0 = A_0 y_0(t) \quad (15)$$

where $A_0 \in \mathbb{R}_{N \times N}$ is the Lyapunov stable and $y_0 = [V_{\text{nom}} \ 0]^T$, and $A_0 = A - BK_{0V}$, with $K_{0V} \in \mathbb{R}_{N \times N}$.

3.2 Proposed distributed control law

Consider a networked MAS with N agents, where each DG unit represents an agent. Assume the measured state is corrupted with noise and that compromises of voltage and frequency can be given as

$$\tilde{y}_{iV}(t) = y_{iV}(t) + \delta_i(t), \quad i = 1, \dots, N \quad (16)$$

where $\tilde{y}_{iV}(t) \in \mathbb{R}_{N \times N}, t \geq 0$, and $\delta_i(t) \in \mathbb{R}_{N \times N}, t \geq 0$ is the noise uncertainty. The noise is assumed to be a white noise, i.e. a zero mean Gaussian noise with variance σ^2 .

Remark 1: If $\delta_i(t)$ is zero, the received state information $\tilde{y}_{iV}(t) = y_{iV}(t), t \geq 0$, and the correct information is available to the local controller of the i th DG unit, else the corrupted state information of voltage signal is available to the controller of the i th DG unit.

For $\delta_i(t) \neq 0$, the objective is to design the distributed secondary noise-resilient voltage control law for i th DG unit such that $\lim_{t \rightarrow \infty} y_{iV}(t) = y_0, \forall i = \{1, \dots, N\}$. For simplicity, we use y_i in place of y_{iV} . The auxiliary voltage control input can be designed as follows [30]:

$$u_i^V = -K_{0V} \tilde{y}_i(t) - \alpha_V K_V \left[\sum_{j \in \mathcal{N}_i} (\tilde{y}_j(t) - \tilde{y}_j(t)) + b_i(\tilde{y}_i(t) - y_0(t)) \right] + v_i^V(t) \quad (17)$$

where $v_i^V(t) \in \mathbb{R}_{N \times N}, t \geq 0$ is the auxiliary corrective control input to counterbalance the impact of noise $\delta_i(t), t \geq 0$. Now the auxiliary

corrective control input is designed for each DG unit in such a way that the ideal system performance can be achieved and the DG voltage will synchronise to the nominal value. Assuming the noise is time invariant, i.e. $\delta_i(t) = \delta_i, i = 1, \dots, N, t \geq 0$.

The corrective voltage control input $v_i^V(t)$ is designed as follows [30]:

$$v_i^V(t) = K_{0V} \hat{\delta}_i(t) + \alpha_V K_V \left[\sum_{j \in \mathcal{N}_i} (\hat{\delta}_i(t) - \hat{\delta}_j(t)) + b_i(\hat{\delta}_i(t)) \right] \quad (18)$$

where

$$\dot{\hat{\delta}}_i = -\beta_V A^T P (\tilde{y}_i(t) - \hat{y}_i(t) - \hat{\delta}_i(t)), t \geq 0 \quad (19)$$

$$\dot{\hat{y}}_i(t) = A_0 \hat{y}_i(t) - \alpha_V B K_V \left[\sum_{j \in \mathcal{N}_i} (\hat{y}_i(t) - \hat{y}_j(t)) + b_i(\hat{y}_i(t) - y_0(t)) \right] + (\beta_V A^T P + \gamma_V I_N) \times (\tilde{y}_i(t) - \hat{y}_i(t) - \hat{\delta}_i(t)), t \geq 0 \quad (20)$$

with $\beta_V \in \mathbb{R}_+$ and $\gamma_V \in \mathbb{R}_+$ are the design parameters; $\hat{\delta}_i(t)$ and $\hat{y}_i(t)$ are the estimates of noise uncertainty $\delta_i(t)$ and compromised state vector $\tilde{y}_i(t)$, respectively; $P \in \mathbb{P}_N$ is the solution of linear matrix inequality given as

$$I_N \otimes (A_0^T P + P A_0 - 2\gamma_V P) - \alpha_V \mathcal{F}_{\mathcal{G}} \otimes (K_V^T B^T P + P B K_V) < 0 \quad (21)$$

Theorem 1: Consider a networked MAS with N DG unit on a connected undirected graph \mathcal{G} , with dynamics of each DG unit is given by (14). The local controller designed in (17) along with the auxiliary corrective control input in (18) forms a Lyapunov stable system and the DG output voltage magnitude V_i synchronises to V_{nom} , irrespective of the stochastic noisy communication links.

Proof: To prove Theorem 1, first we obtain the compact form of the designed controller in (15). By (14) and (17), we can write

$$\dot{y}_i(t) = Ay_i(t) - BK_{0V} y_i(t) - \alpha_V B K_V \left[\sum_{j \in \mathcal{N}_i} (y_j(t) - y_j(t)) + b_i(y_i(t) - y_0(t)) \right] - \alpha_V B K_V \times \sum_{j \in \mathcal{N}_i} (\delta_i - \delta_j) - B(\alpha_V b_i K_V + K_{0V}) \delta_i + B v_i^V(t) \quad (22)$$

Now, assume $y(t) = [y_1^T(t), \dots, y_N^T(t)]^T$, $\delta = [\delta_1^T, \dots, \delta_N^T]^T$, and $v^V(t) = [v_1^V(t), \dots, v_N^V(t)]^T$, then (15) can be rewritten in compact form as follows:

$$\begin{aligned} \dot{y}(t) &= [I_N \otimes A_0 - \alpha_V \mathcal{F}_{\mathcal{G}} \otimes BK_V]y(t) \\ &\quad + (\alpha_V G_{\mathcal{G}} \otimes BK_V)y_0(t) \\ &\quad - (I_N \otimes A)\delta + (I_N \otimes B)v^V(t), \quad t \geq 0 \end{aligned} \quad (23)$$

Using (16) and (23) and $\tilde{y}(t) = [\tilde{y}_1^T(t), \dots, \tilde{y}_N^T(t)]^T$, $\tilde{y}(t)$ can be written in compact form as follows:

$$\begin{aligned} \dot{\tilde{y}}(t) &= [I_N \otimes A_0 - \alpha_V \mathcal{F}_{\mathcal{G}} \otimes BK_V]\tilde{y}(t) \\ &\quad + (\alpha_V G_{\mathcal{G}} \otimes BK_V)y_0(t) \\ &\quad - (I_N \otimes A)\delta + (I_N \otimes B)v^V(t), \quad t \geq 0 \end{aligned} \quad (24)$$

Similarly, the compact form of $\hat{y}(t)$, with $\hat{y}(t) = [\hat{y}_1^T(t), \dots, \hat{y}_N^T(t)]^T$, can be written as

$$\begin{aligned} \dot{\hat{y}}(t) &= [I_N \otimes A_0 - \alpha_V \mathcal{F}_{\mathcal{G}} \otimes BK_V]\hat{y}(t) \\ &\quad + (\alpha_V G_{\mathcal{G}} \otimes BK_V)y_0(t) \\ &\quad - (\alpha_V \mathcal{F}_{\mathcal{G}} \otimes BK_V + I_N \otimes BK_0)\hat{\delta} \\ &\quad + (I_N \otimes B)v^V(t) + \psi(t), \quad t \geq 0 \end{aligned} \quad (25)$$

where $\psi(t) = [\psi_1^T(t), \dots, \psi_N^T(t)]^T$, with $\psi_i(t) = -\hat{\delta}_i(t) + \gamma_V e_i(t)$. Define $e_i(t) = \tilde{y}_i(t) - \hat{y}_i(t) - \delta_i(t)$, and $\tilde{\delta}_i(t) = \delta_i - \hat{\delta}_i(t)$, and their respective compact form can be given as

$$\dot{e}(t) = (A_e - \gamma_V I_N)e(t) - (I_N \otimes A)\tilde{\delta}(t), \quad t \geq 0 \quad (26)$$

and

$$\dot{\tilde{\delta}}(t) = (I_N \otimes \beta_V A^T P)e(t), \quad t \geq 0 \quad (27)$$

where $A_e = I_N \otimes A_0 - \alpha_V \mathcal{F}_{\mathcal{G}} \otimes BK_V$ and $e(t) = [e_1^T(t), \dots, e_N^T(t)]^T$, $\tilde{\delta}(t) = [\tilde{\delta}_1^T(t), \dots, \tilde{\delta}_N^T(t)]^T$.

From [30], proving the Lyapunov stability of (17) is equivalent to prove the Lyapunov stability of (26) and (27) in the sense of Lyapunov criterion. Consider a Lyapunov candidate function as

$$\begin{aligned} V(e, \tilde{\delta}) &= \sum_{i=1}^N (e_i^T P e_i + \beta_V^{-1} \tilde{\delta}_i^T \tilde{\delta}_i) \\ &= e^T (I_N P) e + \beta_V^{-1} \tilde{\delta}^T \tilde{\delta} \end{aligned} \quad (28)$$

Differentiating (24) with respect to time along the trajectories of (26) and (28) yields

$$\begin{aligned} \dot{V}(e, \tilde{\delta}) &= e^T (I_N (A_0^T P + P A_0 - 2\gamma_V P) \\ &\quad - \alpha_V \mathcal{F}_{\mathcal{G}} (K_V^T B^T P + P B K_V)) e \leq 0 \end{aligned} \quad (29)$$

Following from [30], it can be shown that $(I_N (A_0^T P + P A_0 - 2\gamma_V P) - \alpha_V \mathcal{F}_{\mathcal{G}} (K_V^T B^T P + P B K_V))$ is Hurwitz. Hence, (26) and (27) are Lyapunov stable for all $(e_0, \tilde{\delta}_0) \in \mathbb{R}_N \times \mathbb{R}_N$. This completes the proof. \square

Remark 2: By Theorem 1 $\lim_{t \rightarrow \infty} \tilde{\delta}(t) = 0$, and $\lim_{t \rightarrow \infty} e(t) = 0$, which implies that $\lim_{t \rightarrow \infty} (y(t) - \hat{y}(t)) = 0$, i.e. the estimate of the state $\hat{y}(t)$, converges to the uncompromised state $y(t)$ for $t \geq 0$. Hence, the proposed control scheme in (17) guarantees the DGs output voltage V_i synchronises to the nominal

value V_{nom} , despite the uncertain noise disturbance in the communication links.

Remark 3: It is important to notice that the voltage control input u_i^V in (17) and the auxiliary corrective control input $v_i^V(t)$ in (18) are independent of the initial conditions of the MG network, and are fully distributed in nature.

4 Noise-resilient frequency synchronisation

In this section, a fully distributed frequency synchronisation scheme is designed in a similar way as in Section 3. Since the active power sharing is provided via droop based primary control level, thus the secondary distributed control scheme should ensure proper active power sharing along with frequency restoration despite the noise uncertainty. Following a similar approach used in Section 3, employing feedback linearisation and transforming the non-linear system dynamics of each DG into a linear system as follows:

$$\dot{y}_{i\omega} = L_{f_i} h_{i\omega} + L_{g_{i\omega}} h_{i\omega} W_i + d_i \dot{W}_i \quad (30)$$

where $L_{f_i} h_{i\omega}$ is the Lie derivative of $h_{i\omega}$ along f_i , $y_{i\omega}$ is the output (ω_i) and W_i is the frequency control input. The first derivative of $y_{i\omega}$ can be written as

$$\dot{y}_{i\omega} = \dot{\omega}_i = \dot{\omega}_{ni} - k_{Pi} \dot{P}_i \quad (31)$$

Define the auxiliary control input as

$$u_i^{\omega} = \dot{\omega}_{ni} - k_{Pi} \dot{P}_i \quad (32)$$

Using (31) and (32) we can write

$$\dot{\omega}_i = u_i^{\omega}, \quad i = \{1, \dots, N\} \quad (33)$$

Now consider the measured frequency states corrupted with noise as follows:

$$\tilde{y}_{i\omega}(t) = y_{i\omega}(t) + \delta_i(t), \quad i = 1, \dots, N \quad (34)$$

The auxiliary frequency control input can be designed as [30]

$$\begin{aligned} u_i^{\omega} &= -K_{0\omega} \tilde{y}_{i\omega}(t) - \alpha_{\omega} K_{\omega} \left[\sum_{j \in \mathcal{N}_i} (\tilde{y}_{i\omega}(t) - \tilde{y}_{j\omega}(t)) \right. \\ &\quad \left. + b_i (\tilde{y}_{i\omega}(t) - y_{0\omega}(t)) \right] + v_i^{\omega}(t) \end{aligned} \quad (35)$$

and the auxiliary corrective control input $v_i^{\omega}(t)$ is designed as follows:

$$\begin{aligned} v_i^{\omega}(t) &= K_{0\omega} \hat{\delta}_i(t) + \alpha_{\omega} K_{\omega} \left[\sum_{j \in \mathcal{N}_i} (\hat{\delta}_i(t) - \hat{\delta}_j(t)) \right. \\ &\quad \left. + b_i (\hat{\delta}_i(t)) \right] \end{aligned} \quad (36)$$

Theorem 2: A distributed noise resilient control scheme designed in (35) and (36) restores the DGs operating frequency ω_i to the nominal frequency ω_{nom} , irrespective of the noise uncertainty in the communication links while guaranteeing accurate real power-sharing.

Proof: The proof can be derived similar to (24)–(29) in Section 3. \square

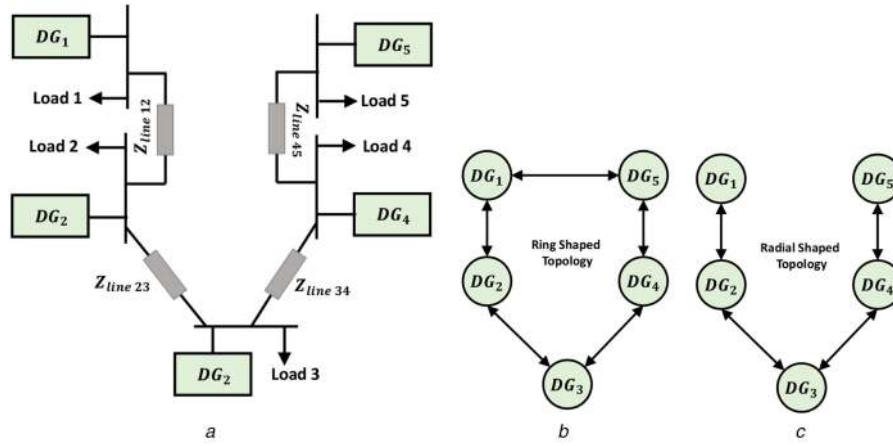


Fig. 4 MG test system
 (a) Single-line diagram of islanded MG test system, (b) Ring communication topology, (c) Radial communication topology

Table 1 Specification of MG test system

	DG 1 and DG 2 and DG 3		DG 4 and DG 5	
DGs	k_Q^V	9.4×10^{-5}	k_Q^V	12.5×10^{-5}
	k_P^{ω}	1.3×10^{-3}	k_P^{ω}	1.5×10^{-3}
	R	0.03Ω	R	0.03Ω
	L	0.35 mH	L	0.35 mH
	R_f	0.1Ω	R_f	0.1Ω
	L_f	1.35 mH	L_f	1.35 mH
	C_f	$50 \mu\text{F}$	C_f	$50 \mu\text{F}$
	K_{PV}	0.1	K_{PV}	0.05
	K_{JV}	420	K_{JV}	390
	K_{PC}	15	K_{PC}	10.5
	K_{IC}	$20,000$	K_{IC}	$16,000$
lines	$Z_{\text{Line}12}$	$Z_{\text{Line}23}$	$Z_{\text{Line}34}$	$Z_{\text{Line}45}$
	$R_l = 0.12 \Omega$	$R_l = 0.175 \Omega$	$R_l = 0.12 \Omega$	$R_l = 0.175 \Omega$
	$L_l = 318 \mu\text{H}$	$L_l = 1847 \mu\text{H}$	$L_l = 318 \mu\text{H}$	$L_l = 1847 \mu\text{H}$

Table 2 MG loads

	Load 1	Load 2	Load 3	Load 4	Load 5
loads	$R = 300 \Omega$	$R = 40 \Omega$	$R = 50 \Omega$	$R = 40 \Omega$	$R = 50 \Omega$
	$L = 477 \text{ mH}$	$L = 64 \text{ mH}$	$L = 64 \text{ mH}$	$L = 64 \text{ mH}$	$L = 95 \text{ mH}$

5 Case studies

The effectiveness of the proposed noise-resilient distributed control scheme is verified by simulating an MG test system shown in Fig. 4a, using MATLAB/SimpowerSystem toolbox. The specifications of DGs, lines, and loads are summarised in Tables 1 and 2, respectively. The performance of the proposed control scheme is evaluated for different noise levels in the communication links and also compared with the conventional method based on neighbourhood tracking error presented in [12] and with a previously reported noise-resilient control approach presented in [27]. This section considers seven cases, namely performance evaluation under load perturbation, plug and play capability, communication network change, performance under different noise level, comparison with the existing conventional and noise resilient method, and performance with communication constraints like delay and data dropout. The considered communication topology is shown in Fig. 4b via an undirected graph. The secondary control parameters are set as follows $\alpha_{\omega} = 200$, $\beta_{\omega} = 80$, $\gamma_{\omega} = 100$, $\alpha_V = 100$, $\beta_V = 40$, $\gamma_V = 80$. The nominal voltage magnitude and operating frequency, and angular frequency are $V_{\text{nom}} = 380 \text{ V}$, $f_{\text{nom}} = 50 \text{ Hz}$, $\omega_{\text{nom}} = 314.16 \text{ rad/s}$, respectively.

5.1 Case 1: Performance evaluation under load perturbation

This subsection studies the performance of the proposed secondary control scheme under the following simulation stages:

1. *Stage 1:* At $t = 0 \text{ s}$, only primary droop control scheme is active.
2. *Stage 2:* At $t = 2 \text{ s}$, proposed noise-resilient secondary control scheme in (17) and (35) are activated.
3. *Stage 2:* At $t = 3 \text{ s}$, an additional load of $R = 30 \Omega$, $L = 47 \text{ mH}$ is connected to load 1.
4. *Stage 2:* At $t = 4 \text{ s}$, load 3 is disconnected from the MG test network.

It is assumed that all communication links are subjected to the same white noise with variance $\sigma^2 = 10^{-2}$ and intrinsic communication link latency of 100 ms. The results are shown in Fig. 5 demonstrate that the proposed noise-resilient control scheme stably restores the voltage and frequency to their nominal values without any deterioration, under small signal disturbance, i.e. load perturbation at $t = 3$, and $t = 4 \text{ s}$. Further, it should be noted that the frequency is a global variable and remains constant throughout the MG, whereas, for proper voltage synchronisation, the reactive power sharing shows mismatches due to line impedance effect

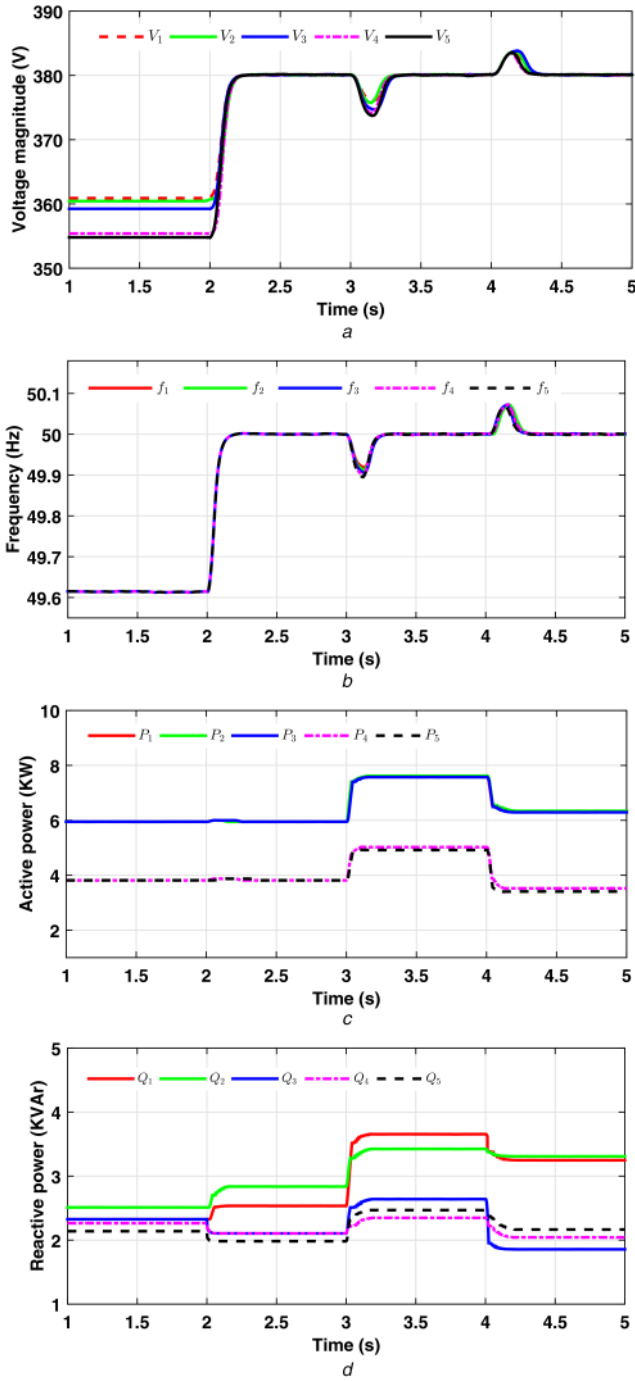


Fig. 5 Performance under load perturbation
(a) DG output voltage magnitude, (b) DG frequency, (c) DG output active power, (d) DG output reactive power

[14]. Therefore, a trade-off between the voltage regulation and reactive power sharing should be made. However, here, we focused mainly on the secondary voltage synchronisation. For accurate reactive power-sharing the virtual-impedance loop can be added along with the secondary control scheme as presented in [32].

5.2 Case 2: Plug and play (PNP) capability

In this subsection, the performance of the proposed control scheme is analysed under PNP scenario. DG 5 is intentionally disconnected from the system at $t = 3$ s, and re-connected at $t = 4$ s. The disconnection of DG 5 causes the communication link 5-4 and link 5-1 breakage as shown in Fig. 6 and the remaining communication links still form a connected graph. Fig. 7 shows that at $t = 3$ s, the power balance is broken and the excess power demand is reallocated among DG 1 to DG 4. Further, at $t = 4$ s, when DG 5 is re-connected to the MG network, the communication topology is

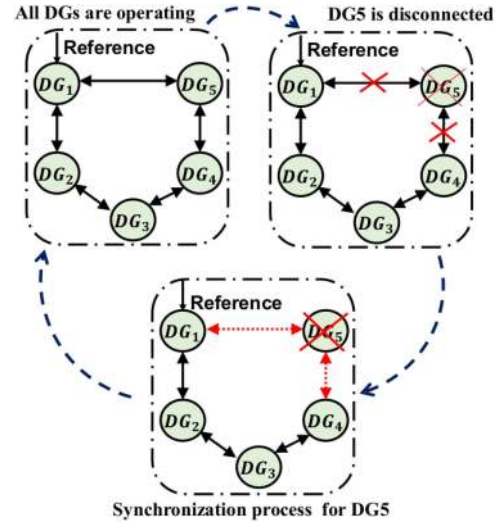


Fig. 6 Communication graph configuration under PNP operation

again updated, and the power-sharing and voltage/frequency regulations are maintained with minimal transients at the disconnection and reconnection points. Therefore, the proposed scheme realises the PNP capability of MG network while providing robust stability and keeping the frequency fluctuations under the maximum allowable limit.

5.3 Case 3: Performance under communication topology change

In this subsection, the performance of the proposed control scheme is analysed with different communication topologies. The communication graph changes from Figs. 4b–c and the same simulation stages are adapted as in Case 1. The results shown in Fig. 8 illustrate that the proposed scheme synchronises the voltage and frequency to their nominal values and shares the active power accurately in the presence of noisy communication links with different communication topologies. Further, the frequency and voltage fluctuations are maintained within the acceptable range during step load perturbations.

5.4 Case 4: Performance with change in noise parameter

In this subsection, the performance of the proposed control scheme is analysed with three different noise variances 10^{-2} , 0.1, and 0.3. The results for voltage and frequency with varying noise levels are shown in Figs. 9 and 10, respectively. It is observed that the voltage and frequency are synchronised within acceptable limits and for $\sigma^2 = 10^{-2}$ and $\sigma^2 = 0.1$. When the noise variance level is increased to $\sigma^2 = 0.3$, the voltage and frequency distortion increases, but are still within acceptable limits. An acceptable limit of maximum frequency deviation of 0.5 Hz is according to ‘IEEE standard for Interconnecting Distributed Resources with Electric Power System Amendment 1’ [33].

Further, the proposed controller performance under varying noise level during simulation is analysed in Figs. 11 and 12. The noise variance varies as follows: $t \leq 2.5$, $\sigma^2 = 10^{-2}$; $2.5 < t \leq 3.5$, $\sigma^2 = 0.1$; $3.5 < t \leq 5$, $\sigma^2 = 0.3$ in Fig. 11, and as $t \leq 2.5$, $\sigma^2 = 0.3$; $2.5 < t \leq 3.5$, $\sigma^2 = 0.1$; $3.5 < t \leq 5$, $\sigma^2 = 10^{-2}$ in Fig. 12. The waveforms shown in Figs. 11 and 12 show that the DGs voltage magnitudes and frequencies are synchronised under acceptable limits for different noise levels. However, for increased noise level $\sigma^2 = 0.3$ the distortion increases a bit but it is still within acceptable limits.

5.5 Case 5: Comparative performance evaluation with method in [12]

In this subsection, we compared the proposed control scheme with the neighbourhood tracking error based controller in [12], and the results are shown in Fig. 13. The results in Figs. 13a and b show

the voltage and frequency waveforms for noise variance $\sigma^2 = 0.1$, for $t \leq 3.5$, and $\sigma^2 = 0.3$, for $t > 3.5$. The voltage and frequency waveforms fluctuate with high-frequency distortions in the case of the conventional approach (when the communication links are subjected to additive noise). However, the proposed control scheme keeps the distortion to the minimum as shown in Figs. 13c and d, and shows desirable performance even if the noise level is tripled at $t = 3.5$ s.

5.6 Comparison with noise resilient control scheme in [27]

In this section, we compared the proposed control scheme with the previously reported noise-resilient secondary control scheme presented in [27]. The simulation results in Figs. 14a and b show the performance comparison between the output voltage magnitude and operating frequency of DG 1 for the proposed control scheme and the control approach in [27] with noise variance $\sigma^2 = 0.1$. It is clear from Figs. 14a and b that the output voltage magnitude and

frequency waveforms fluctuate significantly using the secondary noise-resilient control approach presented in [27]. Also, it takes longer synchronisation time for voltage and frequency. However, the proposed control scheme effectively restores the output voltage magnitude and frequency in comparison with the method presented in [27].

Further, as shown in Figs. 14c and d, the voltage and frequency waveforms fluctuate greatly with high-frequency distortion using the secondary control scheme in [27], whereas, the proposed distributed noise-resilient secondary control scheme as shown in Figs. 13c and d outperforms the controller in [27] in terms of distortions, even if the noise variance is increased threefold, i.e. $\sigma^2 = 0.3$, at $t = 3.5$ s. Hence, the proposed noise-resilient secondary control scheme exhibit robust and superior performance over the noise resilient control approach presented in [27], regarding

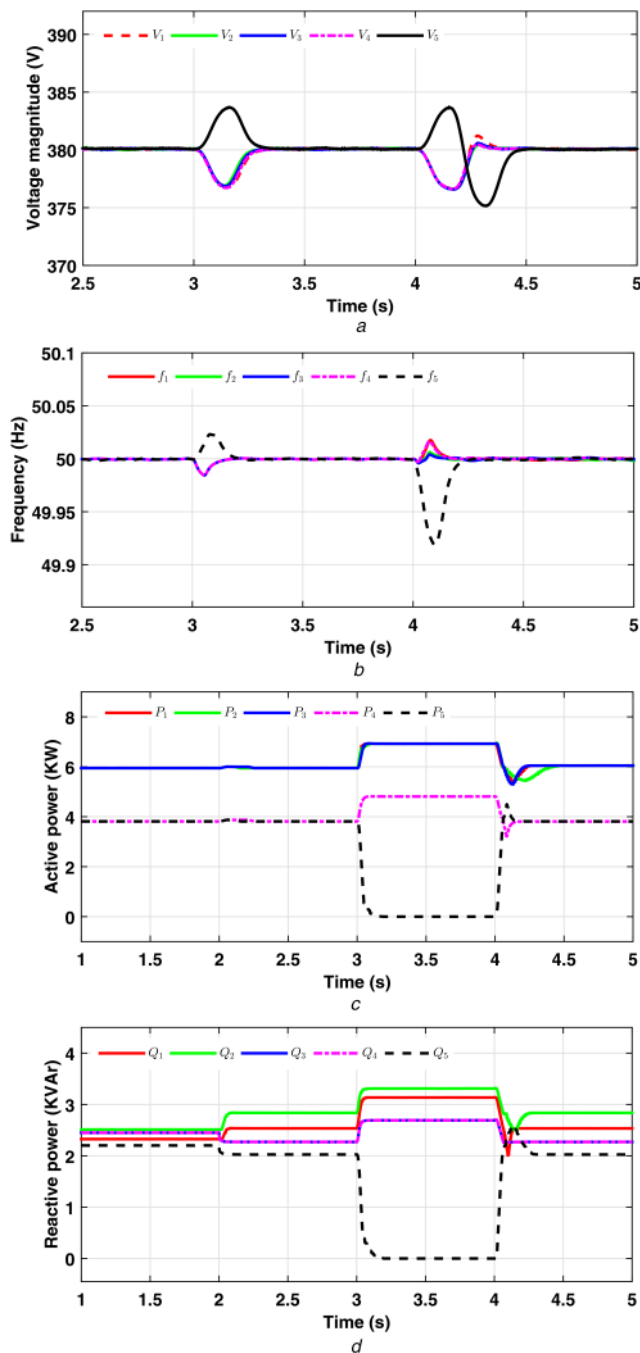


Fig. 7 Performance under PNP operation
(a) DG output voltage magnitude, (b) DG frequency, (c) DG output active power, (d) DG output reactive power

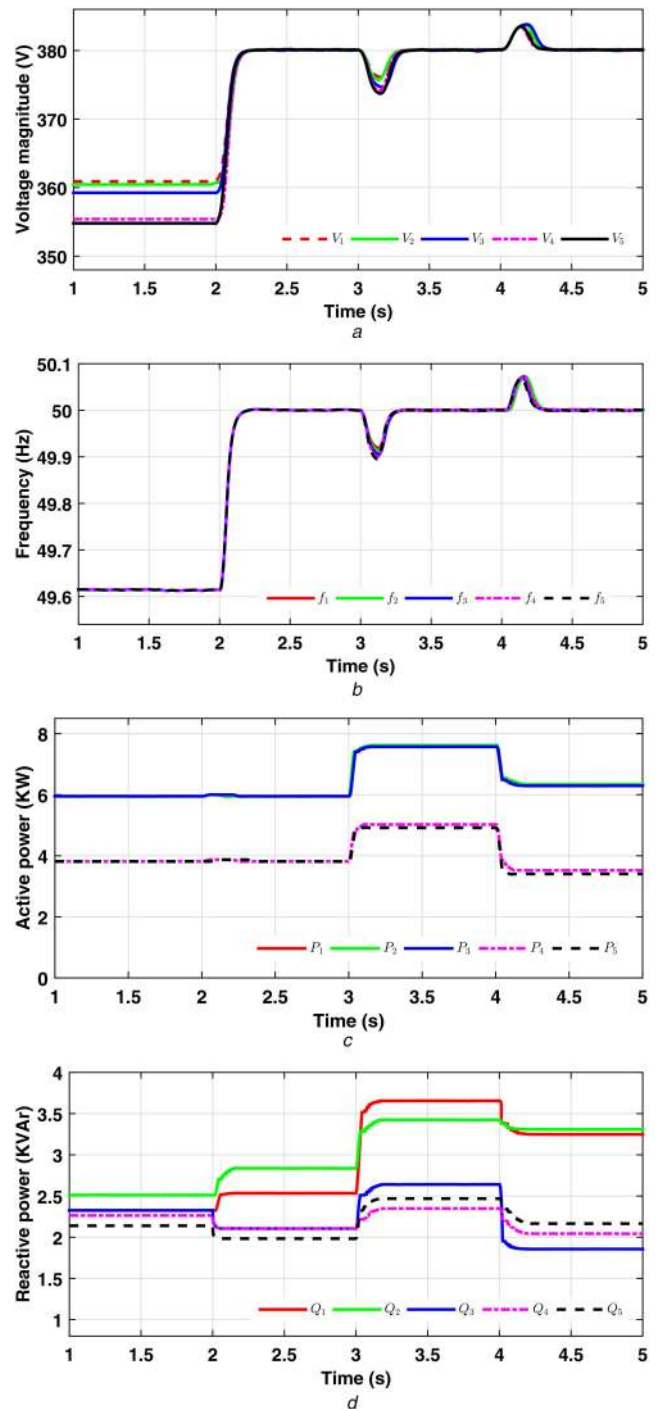


Fig. 8 Performance under radial communication topology
(a) DG output voltage magnitude, (b) DG frequency, (c) DG output active power, (d) DG output reactive power

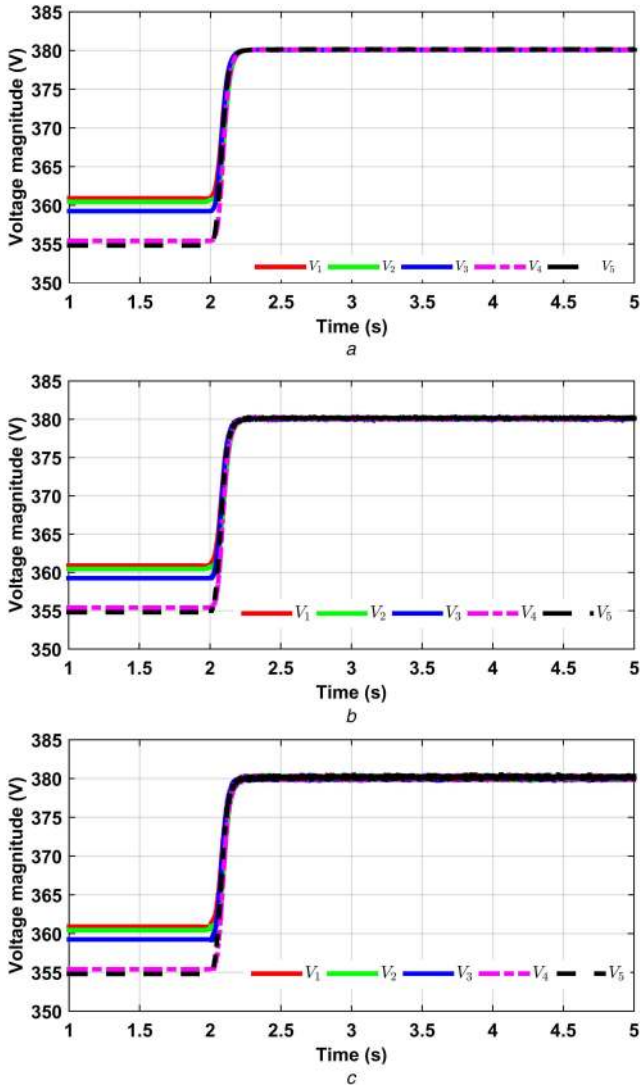


Fig. 9 Voltage restoration in the presence of noise
 (a) DG output voltage magnitude with noise $\sigma^2 = 10^{-2}$, (b) DG output voltage magnitude with noise $\sigma^2 = 0.1$, (c) DG output voltage magnitude with noise $\sigma^2 = 0.3$

restoration time, transients during load perturbation and high-frequency distortions due to noisy communication links.

5.7 Performance with communication latency and data dropout

The communication link has an inherent time latency due to data congestion along with the noisy communication links. The time latency adversely affects the restoration time of the secondary control scheme. Therefore, the impact of the communication link latency is considered in this case to illustrate the performance of the proposed noise-resilient secondary control scheme, along with a noisy communication link having noise variance $\sigma^2 = 0.1$. Here, we considered two different cases of communication link latency (τ_d), i.e. $\tau_d = 1$ s and $\tau_d = 2$ s. The results shown in Figs. 15a and b present the voltage and frequency synchronisation performances of the proposed noise-resilient control scheme for $\tau_d = 1$ s. Next, Figs. 15c and d show the voltage and frequency waveforms for $\tau_d = 2$ s, respectively. The proposed control scheme restores the voltage and frequency with longer restoration time for higher communication link latencies. However, the restoration performance has a negligible impact for $\tau_d = 100$ ms or less.

Further, another communication constraint is data dropout which may occur in communication links and adversely affects the performance of the proposed noise-resilient secondary control scheme. The higher data dropout may lead to significantly larger steady-state error in voltage and frequency terms. In our case study,

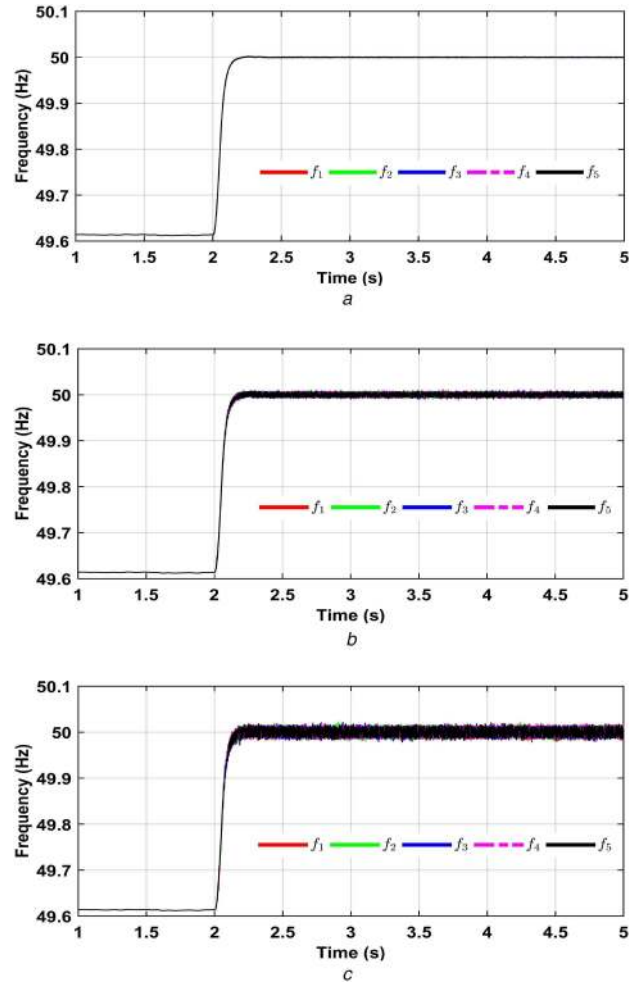


Fig. 10 Frequency restoration in the presence of noise
 (a) DG frequency with noise $\sigma^2 = 10^{-2}$, (b) DG frequency with noise $\sigma^2 = 0.1$, (c) DG frequency with noise $\sigma^2 = 0.3$

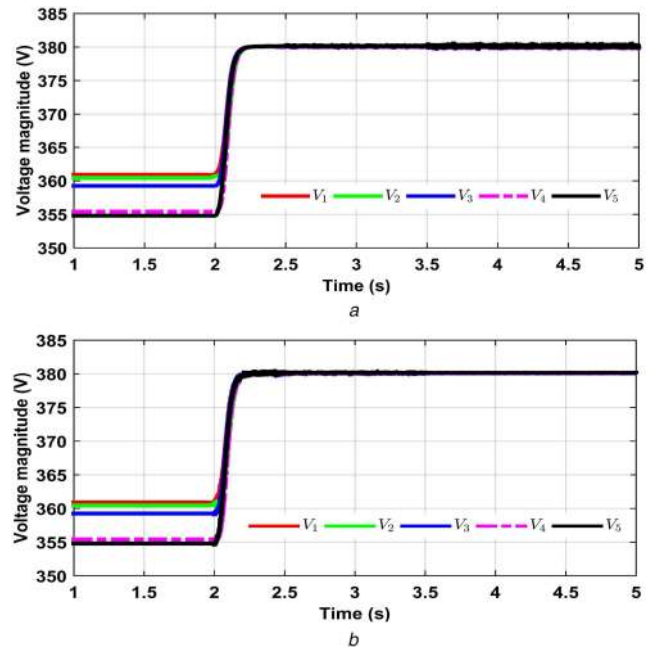


Fig. 11 Voltage restoration in the presence of varying noise
 (a) DG output voltage magnitude with noise $\sigma^2 = 10^{-2}$, $t \leq 2.5$ s; $\sigma^2 = 0.1$, 2.5 s $< t \leq 3.5$ s; $\sigma^2 = 0.3$, 3.5 s $< t \leq 5$ s, (b) DG output voltage magnitude with noise $\sigma^2 = 0.3$, $t \leq 2.5$ s; $\sigma^2 = 0.1$, 2.5 s $< t \leq 3.5$ s; $\sigma^2 = 10^{-2}$, 3.5 s $< t \leq 5$ s

we consider two different cases of packet dropout, first every 30 ms and second every 10 ms in all the communication links, with

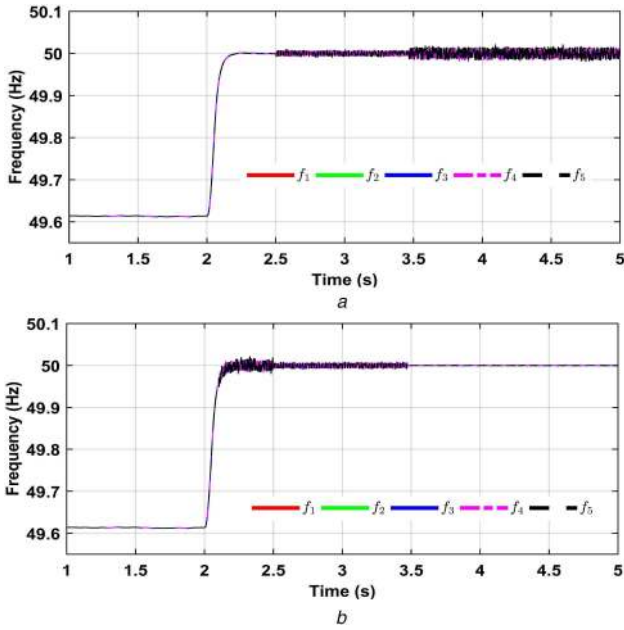


Fig. 12 Frequency restoration in the presence of varying noise
 (a) DG frequency with noise $\sigma^2 = 10^{-2}$, $t \leq 2.5$ s; $\sigma^2 = 0.1$, 2.5 s $< t \leq 3.5$ s; $\sigma^2 = 0.3$, 3.5 s $< t \leq 5$ s, (b) DG frequency with noise $\sigma^2 = 0.3$, $t \leq 2.5$ s; $\sigma^2 = 0.1$, 2.5 s $< t \leq 3.5$ s; $\sigma^2 = 10^{-2}$, 3.5 s $< t \leq 5$ s

100 ms of constant communication link latency. The proposed noise-resilient control scheme exhibits robust performance as shown in Figs. 16a and b under the first case. However, for the second case, the waveform shows negligible transients at the time of voltage and frequency restoration as shown in Figs. 16c and d, which is due to more frequent data drop.

5.8 Results analysis and discussion

The proposed noise resilient secondary control scheme restores the voltage and frequency to their nominal values while accurately sharing the active power among the DG units. The distributed nature of the proposed control scheme eliminates the need for a central controller and thereby obviates the risk of single point failures. We presented DG unit modelling, noise resilient controller design procedure and performance evaluation of the proposed controller for small and large signal disturbances via off-line simulation in MATLAB/Simulink. The control scheme shows robustness against the communication topology change and noise parameter variation. Further, the main achievements obtained from simulation results of the proposed noise-resilient control strategy are

1. Enables the PNP capability of MG network by connecting/disconnecting a DG unit or load without losing system stability.
2. The maximum allowable frequency deviation threshold is of ± 0.5 Hz, according to 'IEEE standard for Interconnecting Distributed Resources with Electric Power System Amendment 1' [34]. The proposed control scheme restores the frequency with small transients (within acceptable limit) while considering noisy measurements.
3. The control approach shows the robust performance by synchronising the voltage and frequency to their nominal values, in the face of un-modelled dynamics, parametric uncertainty, noise parameter variations, load disturbance while maintaining accurate real power-sharing.

6 Conclusions

This paper proposes a distributed secondary control scheme for voltage and frequency synchronisation of an autonomous MG while considering the noisy communication link among the DG units. The proposed noise-resilient scheme is fully distributed and

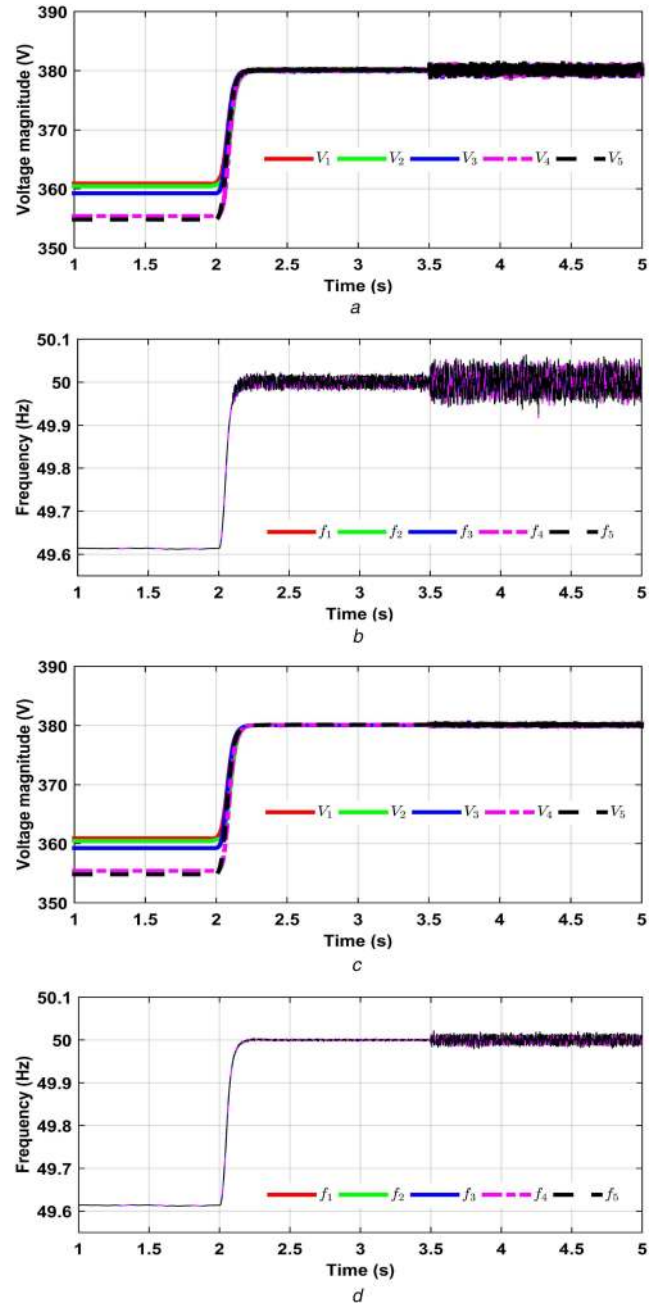


Fig. 13 Comparison of the proposed control scheme with the conventional control approach

(a) DG output voltage magnitude using conventional control scheme, (b) DG frequency using conventional control scheme, (c) DG output voltage magnitude using proposed control scheme, (d) DG frequency using proposed control scheme

considers the complete non-linear dynamics of the MG network. The performance of the proposed control scheme is evaluated for small-signal (step load perturbation) and large-signal disturbances (PNP operation), and changes in communication topology. The impact of different noise level in communication links on the proposed voltage and frequency control scheme is evaluated to verify the robustness of the proposed noise-resilient control scheme. Further, the proposed control scheme is compared with the conventional neighbourhood tracking error based control approach and a previously reported noise-resilient control scheme. The proposed noise-resilient control scheme restores the voltage and frequency and shows less fluctuation with noisy communication links than the conventional one. The control scheme is independent of noise type and the MG system parameters. It should be remarked that the reactive power sharing is not accurate, because of the line impedance effect. The accurate reactive power sharing, while maintaining precise voltage synchronisation is the future research work of the authors.

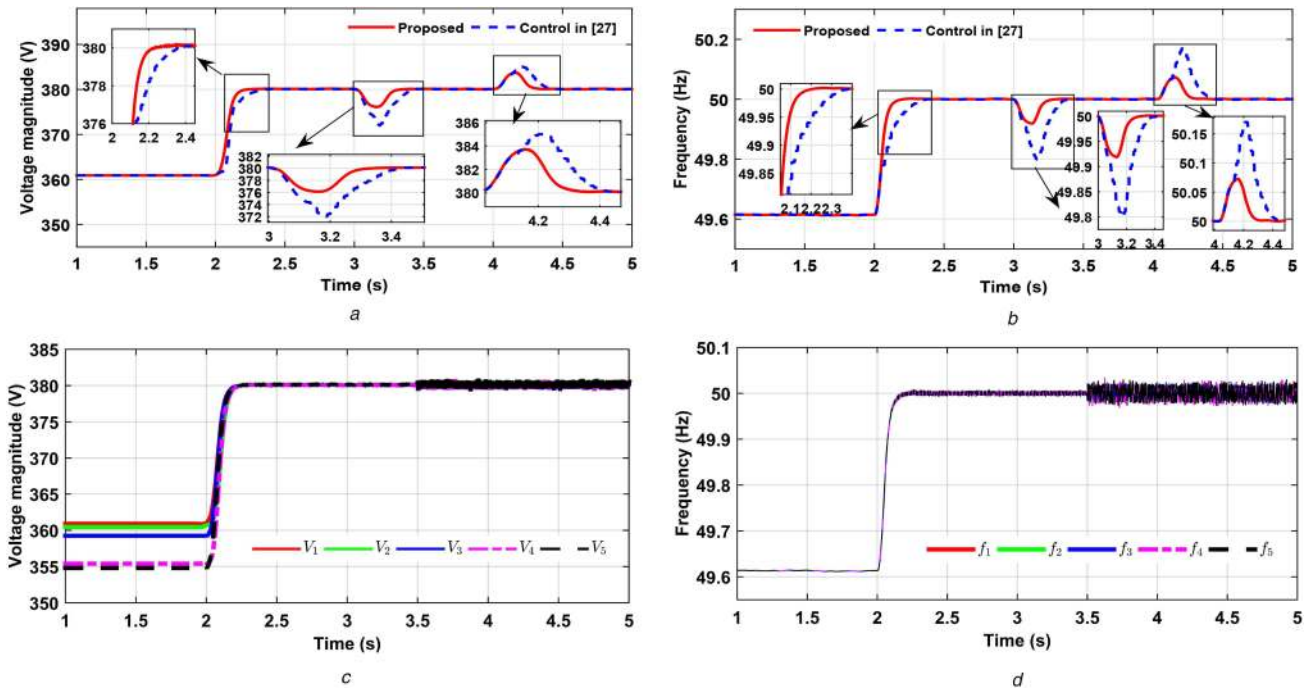


Fig. 14 Comparison of proposed control scheme with the control approach in [27]

(a) Performance comparison with method in [27]: voltage magnitude, (b) Performance comparison with method in [27]: frequency (c) DG output voltage magnitude under control approach in [27], (d) DG output frequency under control approach in [27]

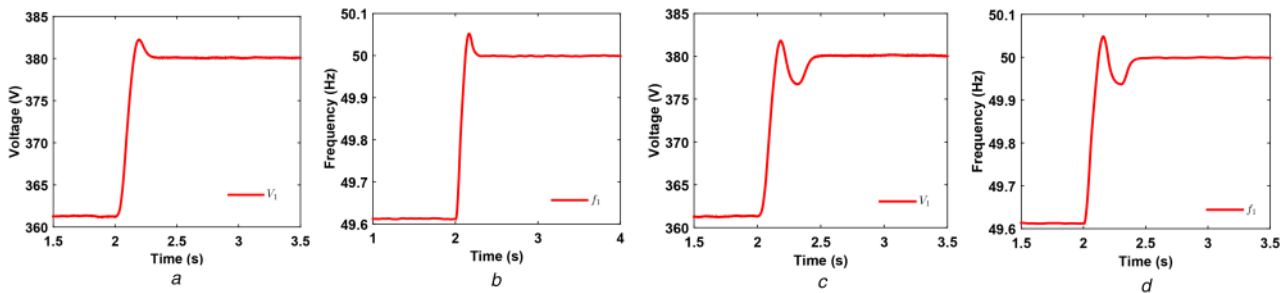


Fig. 15 Performance under communication link latency

(a) Voltage magnitude for latency $\tau_d = 1$ s, (b) Frequency for latency $\tau_d = 1$ s, (c) Voltage magnitude for latency $\tau_d = 2$ s, (d) Frequency for latency $\tau_d = 2$ s

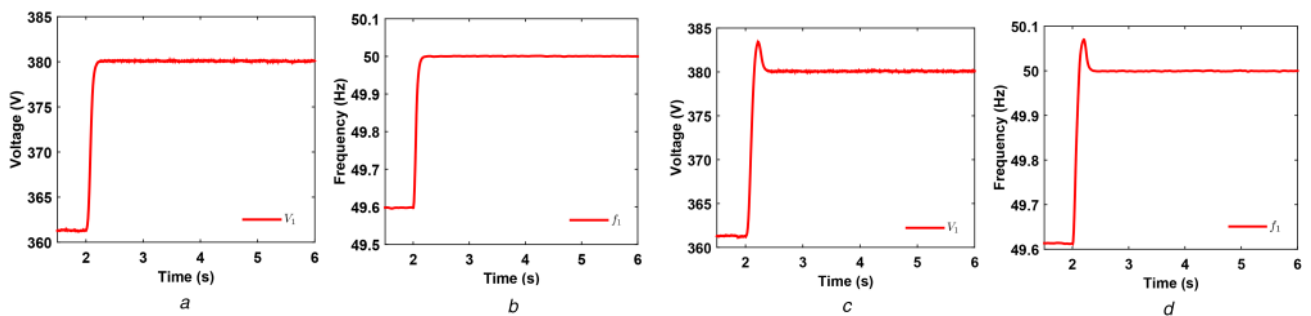


Fig. 16 Performance with data dropout in all links

(a) Voltage magnitude for data dropout every 30 ms, (b) Frequency for data dropout every 30 ms, (c) Voltage magnitude for data dropout every 10 ms, (d) Frequency for data dropout every 10 ms

7 References

- [1] Lopes, J.A.P., Moreira, C.L., Madureira, A.G.: 'Defining control strategies for microgrids islanded operation', *IEEE Trans. Power Syst.*, 2006, **21**, (2), pp. 916–924
- [2] Katiraei, F., Iravani, M.R., Lehn, P.W.: 'Micro-grid autonomous operation during and subsequent to islanding process', *IEEE Trans. Power Deliv.*, 2005, **20**, (1), pp. 248–257
- [3] Olivares, D.E., Mehrizi-Sani, A., Etemadi, A.H., *et al.*: 'Trends in microgrid control', *IEEE Trans. Smart Grid*, 2014, **5**, (4), pp. 1905–1919
- [4] Shrivastava, S., Subudhi, B., Das, S.: 'Distributed voltage and frequency synchronisation control scheme for islanded inverter-based microgrid', *IET Smart Grid*, 2018, **1**, (2), pp. 48–56
- [5] Shrivastava, S., Subudhi, B., Das, S.: 'Consensus-based voltage and frequency restoration scheme for inertia-less islanded microgrid with communication latency'. 2017 IEEE Region 10 Conf. (TENCON 2017), Penang, Malaysia, 2017, pp. 745–750
- [6] Guerrero, J.M., Chandorkar, M., Lee, T.L., *et al.*: 'Advanced control architectures for intelligent microgrids-part I: decentralized and hierarchical control', *IEEE Trans. Ind. Electron.*, 2013, **60**, (4), pp. 1254–1262
- [7] Bidram, A., Davoudi, A.: 'Hierarchical structure of microgrids control system', *IEEE Trans. Smart Grid*, 2012, **3**, (4), pp. 1963–1976
- [8] Guerrero, J.M., Vasquez, J.C., Matas, J., *et al.*: 'Hierarchical control of droop-controlled ac and dc microgrids – a general approach toward standardization', *IEEE Trans. Ind. Electron.*, 2011, **58**, (1), pp. 158–172
- [9] Cady, S.T., Domiguez-Garcia, A.D., Hadjicostis, C.N.: 'A distributed generation control architecture for islanded ac microgrids', *IEEE Trans. Control Syst. Technol.*, 2015, **23**, (5), pp. 1717–1735

- [10] Tan, K., Peng, X., So, P.L., *et al.*: 'Centralized control for parallel operation of distributed generation inverters in microgrids', *IEEE Trans. Smart Grid*, 2012, **3**, (4), pp. 1977–1987
- [11] Vovos, P.N., Kiprakis, A.E., Wallace, A.R., *et al.*: 'Centralized and distributed voltage control: impact on distributed generation penetration', *IEEE Trans. Power Syst.*, 2007, **22**, (1), pp. 476–483
- [12] Bidram, A., Davoudi, A., Lewis, F.L., *et al.*: 'Secondary control of microgrids based on distributed cooperative control of multi-agent systems', *IET Gener. Transm. Distrib.*, 2013, **7**, (8), pp. 822–831
- [13] Bidram, A., Lewis, F.L., Davoudi, A.: 'Distributed control systems for small-scale power networks: using multiagent cooperative control theory', *IEEE Control Syst.*, 2014, **34**, (6), pp. 56–77
- [14] Simpson-Porco, J.W., Shafiee, Q., Dörfler, F., *et al.*: 'Secondary frequency and voltage control of islanded microgrids via distributed averaging', *IEEE Trans. Ind. Electron.*, 2015, **62**, (11), pp. 7025–7038
- [15] Guo, F., Wen, C., Mao, J., *et al.*: 'Distributed secondary voltage and frequency restoration control of droop-controlled inverter-based microgrids', *IEEE Trans. Ind. Electron.*, 2015, **62**, (7), pp. 4355–4364
- [16] Shafiee, Q., Guerrero, J.M., Vasquez, J.C.: 'Distributed secondary control for islanded microgrids – a novel approach', *IEEE Trans. Power Electron.*, 2014, **29**, (2), pp. 1018–1031
- [17] Nasirian, V., Shafiee, Q., Guerrero, J.M., *et al.*: 'Droop-free distributed control for ac microgrids', *IEEE Trans. Power Electron.*, 2016, **31**, (2), pp. 1600–1617
- [18] Bidram, A., Davoudi, A., Lewis, F.L., *et al.*: 'Distributed cooperative secondary control of microgrids using feedback linearization', *IEEE Trans. Power Syst.*, 2013, **28**, (3), pp. 3462–3470
- [19] Lu, X., Yu, X., Lai, J., *et al.*: 'A novel distributed secondary coordination control approach for islanded microgrids', *IEEE Trans. Smart Grid*, 2018, **9**, (4), pp. 2726–2740
- [20] Ahumada, C., Cárdenas, R., Sáez, D., *et al.*: 'Secondary control strategies for frequency restoration in islanded microgrids with consideration of communication delays', *IEEE Trans. Smart Grid*, 2016, **7**, (3), pp. 1430–1441
- [21] Lu, X., Chen, N., Wang, Y., *et al.*: 'Distributed impulsive control for islanded microgrids with variable communication delays', *IET Control Theory Appl.*, 2016, **10**, (14), pp. 1732–1739
- [22] Lai, J., Zhou, H., Lu, X., *et al.*: 'Droop-based distributed cooperative control for microgrids with time-varying delays', *IEEE Trans. Smart Grid*, 2016, **7**, (4), pp. 1775–1789
- [23] Proakis, J.G., Salehi, M., Zhou, N., *et al.*: 'Communication systems engineering', vol. 2 (Prentice-Hall, New Jersey, 1994)
- [24] Hu, J., Feng, G.: 'Distributed tracking control of leader–follower multi-agent systems under noisy measurement', *Automatica*, 2010, **46**, (8), pp. 1382–1387
- [25] Hong, Y., Chen, G., Bushnell, L.: 'Distributed observers design for leader-following control of multi-agent networks', *Automatica*, 2008, **44**, (3), pp. 846–850
- [26] Abhinav, S., Schizas, I.D., Davoudi, A.: 'Noise-resilient synchrony of ac microgrids'. IEEE Resilience Week (RWS, 2015), Philadelphia, PA, USA, 2015, pp. 1–6
- [27] Dehkordi, N.M., Baghaee, H.R., Sadati, N., *et al.*: 'Distributed noise-resilient secondary voltage and frequency control for islanded microgrids', *IEEE Trans. Smart Grid*, 2018
- [28] Fax, J.A., Murray, R.M.: 'Information flow and cooperative control of vehicle formations', *IEEE Trans. Autom. Control*, 2004, **49**, (9), pp. 1465–1476
- [29] Godsil, C., Royle, G.: 'Algebraic graph theory: springer graduate texts in mathematics 207' (Springer-Verlag, New York, 2001)
- [30] Arabi, E., Yucelen, T., Haddad, W.M.: 'Mitigating the effects of sensor uncertainties in networked multi-agent systems', *J. Dyn. Syst. Meas. Control*, 2017, **139**, (4), p. 041003
- [31] Tiwari, R., Deshmukh, S.: 'Prior information based Bayesian MMSE estimation of velocity in Hetnets', *IEEE Wirel. Commun. Lett.*, 2018
- [32] He, J., Li, Y.W., Guerrero, J.M., *et al.*: 'An islanding microgrid power sharing approach using enhanced virtual impedance control scheme', *IEEE Trans. Power Electron.*, 2013, **28**, (11), pp. 5272–5282
- [33] 'IEEE standard conformance test procedures for equipment interconnecting distributed resources with electric power systems - amendment 1'. IEEE Std 15471a-2015 (Amendment to IEEE Std 15471-2005), 2015, pp. 1–27
- [34] Fu, J., Wang, J.Z.: 'Finite-time consensus for multi-agent systems with globally bounded convergence time under directed communication graphs', *Int. J. Control*, 2017, **90**, (9), pp. 1807–1817